Abstracta

Ano XXV - N. 02

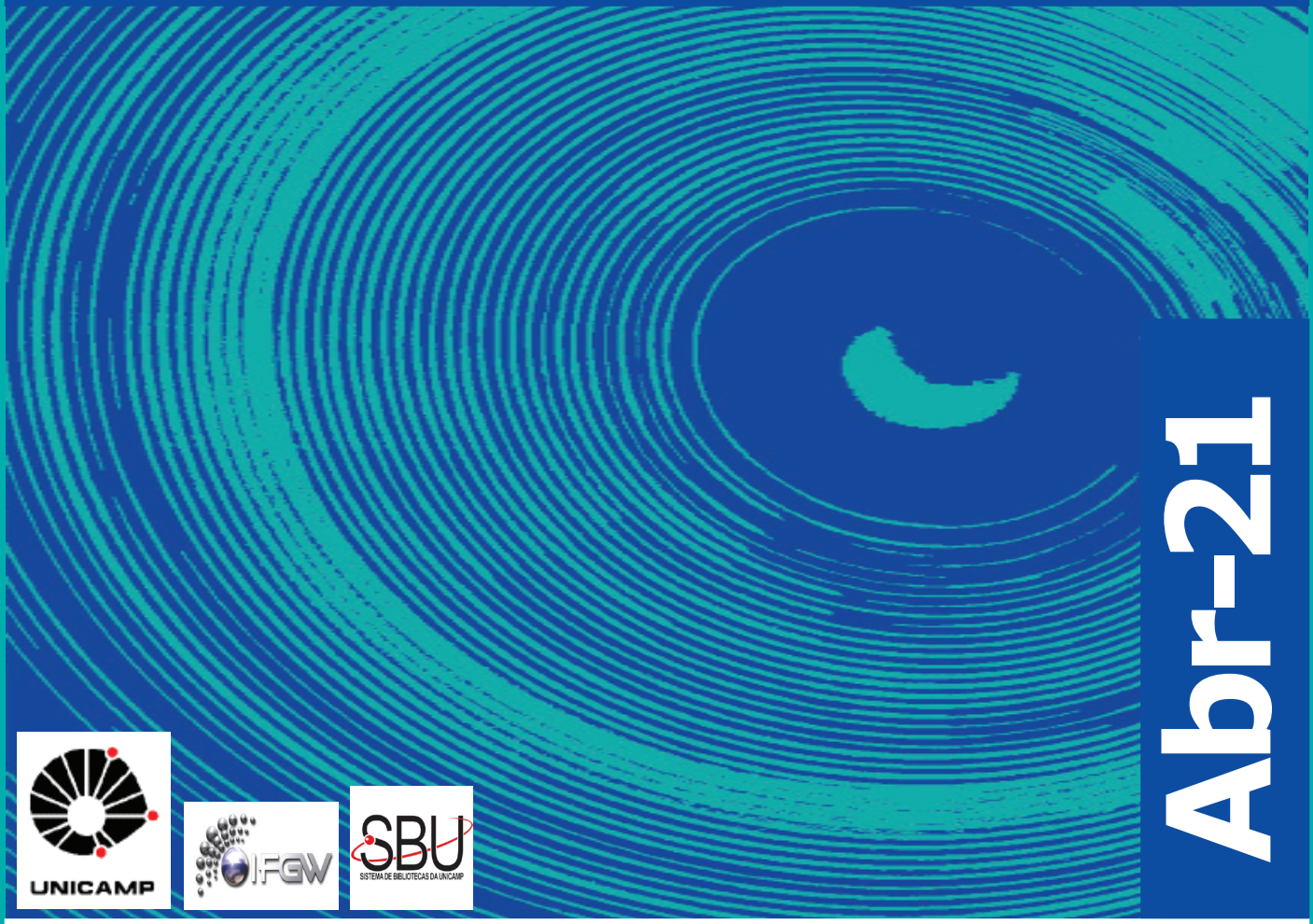

Abr-21

Artigos publicados - P032-2021 à P077-2021

Artigos aceitos para publicação - A001-2021

Correções - Co003-2021 à Co005-2021

Defesas de Dissertações do IFGW - D003-2021 à D008-2021

Defesas de Teses do IFGW - T002-2021 à T003-2021

Defesas de Teses e Dissertações do PECIM - Pe001-2021

Artigos publicados

[P032-2021] "Accurate Image-guided (Re)Placement of NIRS Probes"

Wu, S. T.; Silva, J. A. I. R.; **Novi, S. L.*; Souza, N. G. S. R. de*; Forero, E. J.*; Mesquita, R. C.***

Background and Objective: Functional near-infrared spectroscopy (fNIRS) has become an attractive choice to neuroscience because of its high temporal resolution, ease of use, non-invasiveness, and affordability. With the advent of wearable fNIRS technology, on-the-spot studies of brain function have become viable. However, the lack of within-subject reproducibility is one of the barriers to the full acceptability of fNIRS. To support the validation of the claim that within--subject reproducibility of fNIRS could benefit from accurate anatomical information, we present in this paper a method to develop an image-based system that improves the placement of the sensors on the scalp at interactive rates. Methods: The proposed solution consists of an electromagnetic digitizer and an interactive visualization system that allows monitoring the movements of the digitizer on a real head with respect to the underlying cerebral cortical structures. GPU--based volume raycasting rendering is applied to unveil these structures from the corresponding magnetic resonance imaging volume. Scalp and cortical surface are estimated from the scanned volume to improve depth perception. An alignment algorithm between the real and scanned heads is devised to visually feedback the position of the stylus of the digitizer. Off-screen rendering of the depthmaps of the visible surfaces makes spatial positioning of a 2D interaction pointer possible. Results: We evaluated the alignment accuracy using four to eight anatomical landmarks and found seven to be a good compromise between precision and efficiency. Next, we evaluated reproducibility in positioning five arbitrarily chosen points on three volunteers by four operators over five sessions. In every session, seven anatomical landmarks were applied in the alignment of the real and the scanned head. For the same volunteer, one-way analysis of variance (ANOVA) revealed no significant differences within the five points digitized by the same operator over five sessions (alpha = 0.05). In addition, preliminary study of motor cortex activation by right-hand finger tapping showed the potential of our approach to increase functional fNIRS reproducibility. Conclusions: Results of experiments suggest that the enhancement of the visualization of the location of the probes on the scalp, relative to the underlying cortical structures, improves reproducibility of fNIRS measurements. As further work, we plan to study the fNIRS reproducibility in other cortical regions and in clinical settings using the proposed system.

COMPUTER METHODS AND PROGRAMS IN BIOMEDICINE 200, 105844, 2021. DOI: 10.1016/j.cmpb.2020.1058

[P033-2021] "Centrality dependence of J /ψ and ψ (2S) production and nuclear modification in p-Pb collisions at s NN = 8 . 16 TeV"

Acharya, S.; Acosta, F. T.; Adam, J.; **Albuquerque, D. S. D.; Chinellato, D. D.*; De Souza, R. D.*; Takahashi, J.***; et al.; ALICE Collaboration

The inclusive production of the J/ and psi (2S) charmonium states is studied as a function of centrality in p-Pb collisions at a centre-of-mass energy per nucleon pair <mml:msqrt>sNN</mml:msqrt> = 8.16 TeV at the LHC. The measurement is performed in the dimuon decay channel with the ALICE apparatus in the centre-of-mass rapidity intervals -4.46 < y(cms)< -2.96 (Pb-going direction) and 2.03 < y(cms)< 3.53 (p-going direction), down to zero transverse momentum (p(T)). The J/<psi> and psi (2S) production cross sections are evaluated as a function of the collision centrality, estimated through the energy deposited in the zero degree calorimeter located in the Pb-going direction. The p(T)-differential J/psi production cross section is measured at backward and forward rapidity for several centrality classes, together with the corresponding average < p(T)> and <mml:mfenced close="<right angle bracket>" open="<">pT2</mml:msubsup></mml:mfenced> values. The nuclear effects affecting the production of both charmonium states are studied using the nuclear modification factor. In the p-going direction, a suppression of the production of both charmonium states is observed, which seems to increase from peripheral to central collisions. In the Pb-going direction, however, the centrality dependence is different for the two states: the nuclear modification factor of the J/psi increases from below unity in peripheral collisions to above unity in central collisions, while for the psi (2S) it stays below or consistent with unity for all centralities with no significant centrality dependence. The results are compared with measurements in p-Pb collisions at <mml:msqrt><mml:msub>sNN</mml:msqrt> = 5.02 TeV and no significant dependence on the energy of the collision is observed. Finally, the results are compared with theoretical models implementing various nuclear matter effects.

JOURNAL OF HIGH ENERGY PHYSICS 2, 2, 2021. DOI: 10.1007/JHEP02(2021)002

[P034-2021] "Constraining the 3-3-1 model with heavy neutral leptons using (g 2)(mu) and dark matter observables"

Alvarez-Salazar, C. E.*; Peres, O. L. G.*

Models with gauge symmetry SU(3)(c) circle times SU(3)(L) circle times U(1)(N) have different candidates for dark matter, for example, a heavy neutral fermion interacting with standard model particles through different mediators, scalar and vector portals. At the same time, these portals can produce signals in the anomalous magnetic moment of the muon that violate the present bounds on this quantity. Combining the requirement to have a dark matter candidate in the SU(3)(c) circle times SU(3)(L) circle times U(1)(N) model with heavy neutral leptons and to explain the anomalous magnetic moment of the muon we set constraints on the highest symmetry breaking scale of the model. These bounds are competitive with the constraints from LHC and set a favored region that can also be tested in future direct detection experiments, such as the LUX-ZEPLIN (LZ) experiment.

PHYSICAL REVIEW D 103[3], 035029, 2021. DOI: 10.1103/PhysRevD.103.035029

[P035-2021] "Crystalline electrical field effects on powdered RE Cu4Al8 (RE = Tb, Dy, Ho and Er) intermetallic compounds"

Mercena, S. G.; Silva, L. S.; Lora-Serrano, R.; Garcia, D. J.; **Souza, J. C.*; Pagliuso, P. G.***; Duque, J. G. S

In this work, structural and magnetic properties RE Cu4Al8 (RE = Tb, Dy, Ho and Er) family of compounds are reported. Measurements of X-ray diffraction, temperature (T) and magnetic field (H) dependencies of magnetization are presented for each compound. The analysis of X-ray diffraction patterns shows a small variation in a (8.705824-8.734991 angstrom) and c (5.123802-5.135258 angstrom) lattice parameters as a function of the rare earth. The T-dependent magnetic susceptibility reveals the Curie-Weiss-like behavior at high-T evolving to antiferromagnetic transitions at low-T (6 < T-N < 28 K) for all studied materials. Measurements of magnetization as a function of magnetic field show field-induced transitions for RE = Dy, Ho and Er, which present larger magnetic moments, though no magnetic saturation is attained (4.4 < M-max < 7.3 mu B) for none of the studied compounds.

This fact is an indicative of strong crystalline electrical field (CEF) effects. We have conducted a detailed analysis, based on a mean-field spin model, in order to determine the CEF parameters from the macroscopic data of the studied powdered samples. Finally, to show the reliability of our calculations, the obtained CEF energy levels and wave functions are compared with previous CEF studies in single crystalline samples of ErCu4Al8, including results obtained from inelastic neutron scattering data.

INTERMETALLICS 130, 107040, 2021. DOI: 10.1016/j.intermet.2020.107040

[P036-2021] "Effect of Oxygen and Aluminum Incorporation on the Local Structure of GaN Nanowires: Insight from Extended X-ray Absorption Fine Structure Analysis"

Parida, S.; Sahoo, M.; Abharana, N.; **Tromer, R. M.*; Galvão, D. S.***; Dhara, S.

A thorough investigation of local structure, influencing the macroscopic properties of the solid, is of potential interest. We investigated the local structure of GaN nanowires (NWs) with different native defect concentrations synthesized by the chemical vapor deposition technique. Extended X-ray absorption fine structure (EXAFS) analysis and semiempirical and density functional theory (DFT) calculations were used to address the effect of dopant incorporation along with other defects on the coordination number and bond length values. The decrease of the bond length values along preferential crystal axes in the local tetrahedral structure of GaN emphasizes the preferred lattice site for oxygen doping. The preferential bond length contraction is corroborated by the simulations. We have also studied the impact on the local atomic configuration of GaN NWs with Al incorporation. AlxGa1-xN NWs are synthesized via novel ion beam techniques of ion beam mixing and post-irradiation diffusion process. The change in the local tetrahedral structure of GaN with Al incorporation is investigated by EXAFS analysis. The analysis provides a clear understanding of choosing a suitable process for ternary III--nitride random alloy formation. The study of the local structure with the EXAFS analysis is corroborated with the observed macroscopic properties studied using Raman spectroscopy.

JOURNAL OF PHYSICAL CHEMISTRY C 125[5], 3225-3234, 2021. DOI: 10.1021/acs.jpcc.0c10669

[P037-2021] "Equilibrium and desorption studies of the competitive binary biosorption of silver(I) and copper(II) ions on brown algae waste"

Nascimento Junior, W. J. do; **Landers, R.***; Silva, M. G. C. da; Vieira, M. G. A.

Synthetic samples of Ag(I) and Cu(II) cations were treated with acidified dealginated Sargassum filipendula, a modified waste from the thickener industry. Binary isotherms demonstrated a balance of simultaneous chemisorption and physisorption processes, pointing out to the presence of ion-exchange, chelation, and complexation mechanisms along with a preference for 2-plus-charged copper ions. Modified-extended Langmuir, non-competitive Langmuir, and Langmuir-Freundlich models exhibited good fit to the experimental data, indicating the complex interactions among adsorbates, active sites, and other soft metals involved. The initial composition of the samples and the operation temperature demonstrated to influence the selectivity of the process. Maximum biosorption capacities were achieved at 30 degrees C for copper (3.60 mmol g(-1)) and silver (8.67 mmol g(-1)). Na(2)EDTA under acidic conditions was able to retrieve previously biosorbed copper ions selectively and at high rates even at very low concentrations of the chelating agent. HNO3 demonstrated high efficiency in removing silver from the biosorbent surface. It is suggested to recover selectively the metals, not only treating wastewater but also separating them for further purposes. XPS analysis marked the main role played by oxygenated groups in binding the adsorbates and the presence of Ag(I) and Cu(I) after the process could be detected. Copper reduction indicated chemical interactions and polarization effects due to the alginate net and elemental silver presence could not be discarded.

JOURNAL OF ENVIRONMENTAL CHEMICAL ENGINEERING 9[1], 104840, 2021. DOI: 10.1016/j.jece.2020.104840

[P038-2021] "Evidence for Higgs boson decay to a pair of muons"

Sirunyan, A. M.; Tumasyan, A.; Adam, W.; **Chinellato, J. A.*; Tonelli Manganote, E. J.***; et al.; CMS Collaboration

Evidence for Higgs boson decay to a pair of muons is presented. This result combines searches in four exclusive categories targeting the production of the Higgs boson via gluon fusion, via vector boson fusion, in association with a vector boson, and in association with a top quark-antiquark pair. The analysis is performed using proton-proton collision data at root s = 13 TeV, corresponding to an integrated luminosity of 137 fb(-1), recorded by the CMS experiment at the CERN LHC. An excess of events over the back- ground expectation is observed in data with a significance of 3.0 standard deviations, where the expectation for the standard model (SM) Higgs boson with mass of 125.38 GeV is 2.5. The combination of this result with that from data recorded at root s = 7 and 8 TeV, corresponding to integrated luminosities of 5.1 and 19.7 fb(-1), respectively, increases both the expected and observed significances by 1%. The measured signal strength, relative to the SM prediction, is 1.19(-0.39)(+0.40)(stat)(-0.14)(+0.15). This result constitutes the first evidence for the decay of the Higgs boson to second generation fermions and is the most precise measurement of the Higgs boson coupling to muons reported to date.

JOURNAL OF HIGH ENERGY PHYSICS 1, 148, 2021. DOI: 10.1007/JHEP01(2021)148

[P039-2021] "Feasibility of 3D printed Co-Cr alloy for dental prostheses applications"

Presotto, A. G. C.; Cordeiro, J. M.; Presotto, J. G. C.; Rangel, E. C.; Cruz, N. C. da; **Landers, R.*;** Barao, V. A. R.; Mesquita, M. F.

The aim of this study was to characterize the surface, microstructural, mechanical, and electrochemical properties of Selective Laser Melting (SLM) 3D-printed Co-Cr alloy when compared with casting and Soft Metal Block (SMB) milling techniques for dental prostheses applications. Specimens with specific dimensions were fabricated by cast, SMB, and SLM technologies with their respective commercially available Co-Cr alloys. Several techniques were carried out to characterize the specimens in terms of surface morphology, chemical composition, microstructure, surface free energy, and mechanical properties. Metal-ceramic bond strength was evaluated with the 3-point bend test. Standard electrochemical tests were conducted in artificial saliva (pH of 6.5). Data were evaluated at a significance level of 5%. Similar microstructure patterns (gamma-phases and epsilon-phases), surface morphology, roughness, and surface free energy were observed among groups ($p > 0.05$, ANOVA). The elemental composition provided by energy-dispersive spectroscopy confirmed the manufacturer's information on the alloys used. SLM technology provided a fine-grained homogeneous and less porous microstructure. Xray photoelectron spectroscopy analysis suggested a thicker oxide film on SLM surfaces.

Highest values of Vickers microhardness, flexural strength, elastic modulus, and metal-ceramic bond strength were found for the SLM group ($p < 0.05$, Tukey's HSD test). The SLM group displayed greater electrochemical stability, presenting higher polarization resistance (Rp(tot)), corrosion potential (E--corr), and pitting potential (E-pit) values ($p < 0.05$, Tukey's HSD test). SLM technology revealed feasible surface, microstructural, mechanical, and electrochemical properties and can be a promising option for the fabrication of dental prostheses.

JOURNAL OF ALLOYS AND COMPOUNDS 862, 158171, 2021. DOI: 10.1016/j.jallcom.2020.158171

[P040-2021] "Fluctuating relativistic hydrodynamics from Crooks theorem"

Torrieri, G.*

We use the Crooks fluctuation theorem [1, 2] together with Zubarev hydro- dynamics [3] to develop a bottom-up theory of hydrodynamic fluctuations. We also use thermodynamic uncertainity relations to estimate bottom-up limits to dissipative transport coefficients.

JOURNAL OF HIGH ENERGY PHYSICS 2, 175, 2021. DOI: 10.1007/JHEP02(2021)175

[P041-2021] "Gluon dynamics from an ordinary differential equation"

Aguilar, A. C.*; Ferreira, M. N.*; Papavassiliou, J.

We present a novel method for computing the nonperturbative kinetic term of the gluon propagator from an ordinary differential equation, whose derivation hinges on the central hypothesis that the regular part of the three-gluon vertex and the aforementioned kinetic term are related by a partial Slavnov-Taylor identity. The main ingredients entering in the solution are projection of the three-gluon vertex and a particular derivative of the ghost-gluon kernel, whose approximate form is derived from a Schwinger-Dyson equation. Crucially, the requirement of a pole-free answer determines the initial condition, whose value is calculated from an integral containing the same ingredients as the solution itself. This feature fixes uniquely, at least in principle, the form of the kinetic term, once the ingredients have been accurately evaluated. In practice, however, due to substantial uncertainties in the computation of the necessary inputs, certain crucial components need be adjusted by hand, in order to obtain self-consistent results. Furthermore, if the gluon propagator has been independently accessed from the lattice, the solution for the kinetic term facilitates the extraction of the momentum-dependent effective gluon mass. The practical implementation of this method is carried out in detail, and the required approximations and theoretical assumptions are duly highlighted.

EUROPEAN PHYSICAL JOURNAL C 81[1], 54, 2021. DOI: 10.1140/epjc/s10052-021-08849-8

[P042-2021] "Goos-Hanchen and Imbert-Federov shifts of vortex beams near critics incidence"

Santana, O. J. S.; **Araujo, L. E. E. de***

We investigate the Goos-Hanchen and Imbert-Federov shifts of linearly polarized vortex beams undergoing internal reflection in a glass prism in the critical region of incidence. Beam shifts are numerically calculated based on a wavenumber-space representation. The influences of the beam's topological charge, angle of incidence, and propagation distance on the beam shifts are investigated. We find that in the critical region, the Goos--Hanchen and Imbert-Federov shifts are coupled by the vortex beam's orbital angular momentum. While the Goos--Hanchen increases with propagation distance, the Imbert--Federov shift is invariant with propagation. We show that both shifts exhibit a dependence on the beam's topological charge beyond a simple linear proportionality.

JOURNAL OF THE OPTICAL SOCIETY OF AMERICA B-OPTICAL PHYSICS 38[2], 300-305, 2021. DOI: 10.1364/JOSAB.410683

[P043-2021] "Grain-Boundary Sliding in Ice I-h: Tribology and Rheology at the Nanoscale"

Ribeiro, I. de A.*; Koning, M. de*

Using nonequilibrium molecular dynamics simulations, we investigate the process of grain-boundary (GB) sliding in ice I-h. We focus on the Sigma 35 symmetric tilt boundary, which has been observed experimentally in polycrystalline samples, and employ the explicit-proton TIP4P/Ice model to describe the interactions between the water molecules. In all cases, the sliding process closely resembles that observed in viscoelastic substances. After an initial linear elastic regime, the stress--strain response passes through a yield-stress maximum that triggers the onset of rheological response through grain sliding, followed by a final relaxation toward a stationary sliding regime. To assess the role of the molecular structure and dynamics of the GB region, we impose various sliding velocities and directions, as well as appraise different temperatures. In particular, we contrast two cases: one in which the GB interface features the presence of a liquid-like layer at 250 K and another in which there is not, at 150 K. In all cases, we find that the liquid--like layer significantly facilitates GB sliding, acting as a boundary lubricant. Both the yield stress as well as the steady-state stress required to maintain sliding, which can be interpreted in terms of effective static and dynamic frictional forces, respectively, are significantly lower than those obtained at 150 K. Whereas in the latter case, the GB region undergoes large-scale amorphization in the frictional process; the thickness of the liquid-like layer at 250 K only increases moderately, reflecting its effectiveness in facilitating the sliding process. The present results provide valuable information regarding the viscous relaxation processes and the role of the disordered GB layer in the frictional behavior at the nanoscale during GB sliding in ice I-h.

JOURNAL OF PHYSICAL CHEMISTRY C 125[1], 627-634, 2021. DOI: 10.1021/acs.jpcc.0c10032

[P044-2021] "Induced magnetization in Cu atoms at the Fe-Co/Cu3Au(001) interface: X-ray magnetic circular dichroism experiments and theoretical results"

Parreiras, S. O.; **Cabral, L. A.***; Lourenco, R. V.; Cotta, A. A. C.; Schio, P.; Cezar, J. C.; Gastelois, P. L.; **Silva, E. Z. da***; Macedo, W. A. A.

The induced magnetization in Cu atoms at the interface between ferromagnetic (FM) Fe/Co ultrathin films and a nonmagnetic (NM) Cu3Au(001) substrate was explored by the investigation of two structures of five alternated Fe and Co monoatomic layers with different stacking orders with a Fe or a Co layer in direct contact with the Cu3Au (001) surface. First principles calculations were applied to disentangle the origin of magnetic proximity effects at these FM/NM interfaces. The hybridization between the electronic states of the FM layers, resulting in a pronounced widening of the d-bands of the local density of states of Fe-Co interface atoms, has a fundamental effect in the spin-polarization of the NM substrate.

X-ray magnetic circular dichroism measurements at the L-2,L-3--edges of Fe, Co and Cu allowed to extract the spin and orbital magnetic moments of Fe and Co, and to measure extremely low magnetic moments induced in Cu atoms. It is shown that the magnetism is induced only in the Cu and Au atoms at the first CuAu monolayer at the very surface of the substrate, i.e., the Cu XMCD signal is due to only 0.5 ML magnetic Cu atoms.

APPLIED SURFACE SCIENCE 548, 149215, 2021. DOI: 10.1016/j.apsusc.2021.149215

[P045-2021] "Iron oxide nanoparticles obtained from steel waste recycling as a green alternative for Congo red dye fast adsorption"

Borth, K. W.; **Galdino, C. W.***; Teixeira, V. de C.; Anaissi, F. J.

Iron oxides can be applied as adsorbents to remove harmful substances from the water used in the textile process. If these oxides can be synthetized through acid digestion of ferrous metal compounds, they can create a cycle of pollutants control from pollutant materials. In this study, two iron oxides were synthetized from steel waste, through razor blades (RB) and bottle caps (BC) acid digestion followed by coprecipitation, for application as Congo red dye adsorbent. Studies about the structure, composition and materials' properties were obtained through x-ray fluorescence, x-ray diffractometry, x-ray absorption, Fourier transform infrared spectroscopy, Raman spectroscopy, thermogravimetric analysis, UV-Vis electronic spectroscopy, nanoparticle tracking analysis, zeta potential and Brunauer, Emmett, Teller method. The structural and composition analysis showed a mixture of iron oxide phases and nanometric average particle sizes. The oxides presented maximum adsorption capacity (q(max)) of 418.41 mg.g(-1) for IO-RB, and 104.17 mg.g(-1) to IO-BC, at mom temperature. Furthermore, the particles present magnetic properties from the produced iron oxide that facilitates their removal from the system, after application. The adsorbents were characterized after adsorption through the same initial techniques; thus, the produced compounds and the adsorption capacity of each oxide were correlated.

APPLIED SURFACE SCIENCE 546, 149126, 2021. DOI: 10.1016/j.apsusc.2021.149126

[P046-2021] "Measurement of the inclusive and differential Higgs boson production cross sections in the leptonic WW decay mode at p root s=13 TeV"

Sirunyan, A. M.; Tumasyan, A.; Adam, W.; **Chinellato, J. A.*; Tonelli Manganote, E. J.***; et al.; CMS Collaboration

Measurements of the fiducial inclusive and differential production cross sections of the Higgs boson in proton-proton collisions at root s = 13 TeV are performed using events where the Higgs boson decays into a pair of W bosons that subsequently decay into a final state with an electron, a muon, and a pair of neutrinos. The analysis is based on data collected with the CMS detector at the LHC during 2016-2018, corresponding to an integrated luminosity of 137 fb(-1). Production cross sections are measured as a function of the transverse momentum of the Higgs boson and the associated jet multiplicity. The Higgs boson signal is extracted and simultaneously unfolded to correct for selection efficiency and resolution effects using maximum-likelihood fits to the observed distributions in data. The integrated fiducial cross section is measured to be 86.5 +/- 9.5 fb, consistent with the Standard Model expectation of 82.5 +/- 4.2 fb. No significant deviation from the Standard Model expectations is observed in the differential measurements.

JOURNAL OF HIGH ENERGY PHYSICS 3, 3, 2021. DOI: 10.1007/JHEP03(2021)003

[P047-2021] "Measurements of dihadron correlations relative to the event plane in Au plus Au collisions at root s(NN)=200 GeV"

Agakishiev, H.; Aggarwal, M. M.; Ahammed, Z.; **Souza, R. D. de*; Takahashi, J.*; Vasconcelos, G. M. S.***; et al.; STAR Collaboration

Dihadron azimuthal correlations containing a high transverse momentum (p(T)) trigger particle are sensitive to the properties of the nuclear medium created at RHIC through the strong interactions occurring between the traversing parton and the medium, i.e. jet-quenching. Previous measurements revealed a strong modification to dihadron azimuthal correlations in Au+Au collisions with respect to p+p and d+Au collisions. The modification increases with the collision centrality, suggesting a path-length or energy density dependence to the jet-quenching effect. This paper reports STAR measurements of dihadron azimuthal correlations in mid-central (20%-60%) Au+Au collisions at root s(NN)= 200 GeV as a function of the trigger particle's azimuthal angle relative to the event plane, phi(s) = vertical bar phi(t) - psi(EP)vertical bar .The azimuthal correlation is studied as a function of both the trigger and associated particle p(T). The subtractions of the combinatorial background and anisotropic flow, assuming Zero Yield At Minimum (ZYAM), are described. The correlation results are first discussed with subtraction of the even harmonic (elliptic and quadrangular) flow backgrounds. The away-side correlation is strongly modified, and the modification varies with phi(s), with a double-peak structure for out-of-plane trigger particles. The near-side ridge (long range pseudo-rapidity Delta(eta) correlation) appears to drop with increasing phi(s) while the jet-like component remains approximately constant. The correlation functions are further studied with the subtraction of odd harmonic triangular flow background arising from fluctuations. It is found that the triangular flow, while responsible for the majority of the amplitudes, is not sufficient to explain the phi(s)-dependence of the ridge or the away--side double-peak structure. The dropping ridge with phi(s), could be attributed to a phi(s)-dependent elliptic anisotropy; however, the physics mechanism of the ridge remains an open question. Even with a phi(s)-dependent elliptic flow, the away-side correlation structure is robust. These results, with extensive systematic studies of the dihadron correlations as a function of phi(s), trigger and associated particle p(T), and the pseudo-rapidity range Delta(eta), should provide stringent inputs to help understand the underlying physics mechanisms of jet-medium interactions in high energy nuclear collisions.

CHINESE PHYSICS C 45[4], 044002, 2021. DOI: 10.1088/1674-1137/abdf3f

[P048-2021] "Measurements of pp -> ZZ production cross sections and constraints on anomalous triple gauge couplings at root s=13 TeV"

Sirunyan, A. M.; Tumasyan, A.; Adam, W.; **Chinellato, J. A.*; Tonelli Manganote, E. J.***; et al.; CMS Collaboration

The production of Z boson pairs in proton-proton (pp) collisions, pp -> (Z/gamma*)(Z/gamma*) -> 2l2l', where l, l' = e or mu, is studied at a center-of-mass energy of 13 TeV with the CMS detector at the CERN LHC. The data sample corresponds to an integrated luminosity of 137 fb(-1), collected during 2016-2018. The ZZ production cross section, sigma(tot)(pp -> ZZ) = 17.4 +/- 0.3 (stat) +/- 0.5 (syst) +/- 0.4 (theo)+/- 0.3 (lumi) pb, measured for events with two pairs of opposite-sign, same-flavor leptons produced in the mass region 60 < m(l+l-) < 120 GeV is consistent with standard model predictions. Differential cross sections are also measured and agree with theoretical predictions. The invariant mass distribution of the four-lepton system is used to set limits on anomalous ZZZ and ZZ gamma couplings.

EUROPEAN PHYSICAL JOURNAL C 81[3], 200, 2021. DOI: 10.1140/epjc/s10052-020-08817-8

[P049-2021] "Metastable solid He-4 and the possible role of point defects"

Pedroso, V. Z.*; Zampronio, V.*; Vitiello, S. A.*

The metastable phase of solid He-4 and the possible role of point defects in its destabilization are investigated by the introduction of a trial function of the shadow class with an explicit symmetrical kernel. This is a trial function that ensures the possible exchange of atoms and the delocalization of atoms and defects in a very effective manner. We show that the formation energy for vacancies is equal to zero at a pressure P-c = 20 +/- 2 atm, which is in excellent agreement with the experimental observation. The pressure at which a self--interstitial also has a formation energy equal to zero, is in agreement with the density where vacancies have the same property. Formation energies of a He-3 interstitial or a substitutional impurity were estimated. Other properties of interest for systems made from He-4 atoms are estimated and compared with results from the literature whenever available.

JOURNAL OF PHYSICS-CONDENSED MATTER 33[7], 075901, 2021. DOI: 10.1088/1361-648X/abc5d6

[P050-2021] "Monitoring and modeling the deposition of metal nanoparticles on surfaces by impedance"

Hensel, R. C.*; Goncalves, M. H.*; Rodrigues, K. L.*; Oiko, V. T. A.*; Pimentel, V. do L.; Pereira-da-Silva, M. A.; **Hillenkamp, M.*; Riul Junior, A.*; Rodrigues, V.***

The study of metallic nanoparticles (NPs) on surfaces and their properties has become a common subject for a variety of areas. Notably, to exploit the unique intrinsic features of deposited NPs in macroscopic devices, samples with low coverage are required. The electrical characterization techniques have, however, so far been limited to systems near or beyond the percolation limit, when the nanostructure's resistive behavior is dominant. Here we describe the impedance response of interdigitated electrodes (IDE) during Ag NP deposition, from the very beginning up to the percolation limit. Our experiments present two regimes: up to similar to 20% of coverage the capacitance grows linearly with the deposition, increasing abruptly afterward. To understand the experimental data, we propose a model in which the capacitance response is attributed to isolated and agglomerated NPs. Initially, isolated NPs contribute to the capacitive response. Beyond similar to 20% coverage, shielded regions of the IDE due to agglomerated NP islands start to dominate until eventually percolation leads to a predominantly conductive signal. These interpretations are supported by Electron Microscopy and Atomic Force Microscopy. The proposed analysis allows improving the control of the concentration of NP deposited on surfaces systems with low coverage by impedance monitoring.

APPLIED SURFACE SCIENCE 544, 148806, 2021. DOI: 10.1016/j.apsusc.2020.148806

[P051-2021] "New sol-gel-derived magnetic bioactive glass--ceramics containing superparamagnetic hematite nanocrystals for hyperthermia application"

Borges, R.; Mendonca-Ferreira, L.; **Rettori, C.***; Pereira, I. S. O.; Baino, F.; Marchi, J.

Although the three main phases of iron oxide - hematite, maghemite, and magnetite - exhibit superparamagnetic properties at the nanoscale, only maghemite and magnetite phases have been explored in magnetic bioactive glass-ceramics aimed at applications in cancer treatment by hyperthermia. In this work, it is reported for the first time the superparamagnetic properties of hematite nanocrystals grown in a 58S bioactive glass matrix derived from sol-gel synthesis. The glass-ceramics are based on the (100-x)(58SiO(2)-33CaO-9P(2)O(5))-xFe(2)O(3) system (x = 10, 20 and 30 wt%). A thermal treatment leads to the growth of hematite (alpha-Fe2O3) nanocrystals, conferring superparamagnetic properties to the glass-ceramics, which is enough to produce heat under an external alternating magnetic field. Besides, the crystallization does not inhibit materials bioactivity, evidenced by the formation of calcium phosphate onto the glass-ceramic surface upon soaking in simulated body fluid. Moreover, their cytotoxicity is similar to other magnetic bioactive glass-ceramics reported in the literature. Finally, these results suggest that hematite nanocrystals' superparamagnetic properties may be explored in multifunctional glass-ceramics applied in bone cancer treatment by hyperthermia allied to bone regeneration.

MATERIALS SCIENCE & ENGINEERING C-MATERIALS FOR BIOLOGICAL APPLICATIONS 120, 111692, 2021. DOI: 10.1016/j.msec.2020.111692

[P052-2021] "On the mechanical properties of atomic and 3D printed zeolite-templated carbon nanotube networks"

Ambekar, R. S.; **Oliveira, E. F.***; Kushwaha, B.; Pal, V.; Machado, L. D.; Sajadi, S. M.; Baughman, R. H.; Ajayan, P. M.; Roy, A. K.; **Galvao, D. S.***; Tiwary, C. S.

Specific strength (strength/density) is a crucial factor while designing high load-bearing structures for aerospace and defense applications. The strength of the material can be enhanced by blending it with high strength components and/or fillers, but both options have limitations, such as that the materials can still fail due to poor filler and matrix interactions. Therefore, there is a great interest in enhancing the strength of materials by playing with topology/geometry. In this work, we have investigated the mechanical properties of zeolite-templated carbon nanotube networks (CNTnets). Atomic models were used to generate macro models that were 3D printed. The mechanical properties of CNTnets were investigated through fully atomistic molecular dynamics simulations and load-bearing tests. Our results show that several aspects of mechanical behavior proved to be scale-independent. The 3D printed structures were able to support high compressive loads without structural failure. Such complex architectures can be exploited for ultralight aerospace and automotive parts.

ADDITIVE MANUFACTURING 37, 101628, 2021. DOI: 10.1016/j.addma.2020.101628

[P053-2021] "On the Mechanical Properties of Popgraphene-Based Nanotubes: a Reactive Molecular Dynamics Study"

Brandao, W. H. S.; Aguiar, A. L.; Ribeiro, L. A.; **Galvão, D. S.***; Sousa, J. M. de

Carbon-based tubular materials have sparked a great interest in future electronics and optoelectronics device applications. In this work, we computationally studied the mechanical properties of nanotubes generated from popgraphene (PopNTs). Popgraphene is a 2D carbon allotrope composed of 5-8-5 rings. We carried out fully atomistic reactive (ReaxFF) molecular dynamics for PopNTs of different chiralities (on; 0THORN and o0; nTHORN) and/or diameters and at different temperatures (from 300 up to 1200 K).

Results showed that the tubes are thermally stable (at least up to 1200 K). All tubes presented stress/strain curves with a quasi-linear behavior followed by an abrupt drop of stress values. Interestingly, armchair-like PopNTs (o0; nTHORN) can stand a higher strain load before fracturing when contrasted to the zigzag-like ones (on; 0THORN). Moreover, it was obtained that Young's modulus (Y-Mod) (750-900 GPa) and ultimate strength (sUS) (120150 GPa) values are similar to the ones reported for conventional armchair and zigzag carbon nanotubes. YMod values obtained for PopNTs are not significantly temperature-dependent. While the sUS values for the o0; nTHORN showed a quasi-linear dependence with the temperature, the on; 0THORN exhibited no clear trends.

CHEMPHYSCHEM, 2021. DOI: 10.1002/cphc.202000840

[P054-2021] "On the physicochemical origin of nanoscale friction: the polarizability and electronegativity relationship tailoring nanotribology"

Leidens, L. M.; Costa, M. E. H. M. da; Figueroa, N. S.; Barbieri, R. A.; **Alvarez, F.***; Michels, A. F.; Figueroa, C. A.

Friction is a ubiquitous manifestation of nature, and when it is studied at the nanoscale, complex and interesting effects arise from fundamental physical and chemical surface properties. Surprisingly, and probably due to the complexity of nanofriction studies, this aspect has not been completely discussed in prior studies. To fully consider the physicochemical influence in nanoscale friction, amorphous carbon films with different amounts of hydrogen and fluorine were prepared, chemically characterized, and evaluated via lateral force microscopy. Hydrogen and fluorine were selected because although they exhibit different physicochemical properties, both contribute to frictional force reduction. Indeed, to explain the experimental behavior, it is necessary to propose a new damping constant unifying both polarizability (physical) and electronegativity (chemical) properties. The satisfactory agreement between theory and experiments may encourage and enhance deeper discussion and new experiments that take into account the chemical peculiarities of frictional behavior relating to nanoscale elastic regimes.

PHYSICAL CHEMISTRY CHEMICAL PHYSICS 23[4], 2873-2884, 2021. DOI: 10.1039/d0cp06436j

[P055-2021] "Organosulphur-modified biochar: An effective green adsorbent for removing metal species in aquatic systems"

Macedo, C. A.; Gontijo, E. S. J.; Herrera, S. G.; Rangel, E. C.; Komatsu, D.; **Landers, R.***; Rosa, A. H.

Organosulphur-modified biochar (BC) can be used as a green adsorbent for removing potentially toxic metal ions from aqueous solutions. In this study, sugarcane bagasse BCs (produced at pyrolysis temperatures from 300 to 700 degrees C) were modified in a single-step reaction with isothiocyanate. The performance and selectivity of raw and modified BCs for removing Cd2+, Ni2+, Pb2+ and Cr3+ from mono- and multi--element aqueous solutions were investigated. The characterisation of the BCs was performed by proximate analysis, Fourier transformed infrared spectroscopy (FTIR), X-ray photoelectron spectroscopy (XPS), energy dispersive spectroscopy (EDS) and pyrolysis coupled to gas chromatography-mass spectrometry (Py-GC-MS). The results showed that the organosulphur modification increased S and N contents on the surface of the BCs, particularly isothiocyanate groups. The maximal adsorptions were observed for raw and modified BCs produced at 700 degrees C and pH 6. The adsorption kinetics of Cd2+, Ni2+, Pb2+ and Cr3+ before and after BC modification was best described by the pseudo-second order kinetic model. The results indicated that the removal of metal ions by modified-biochars follows the order Pb2+ > Cr3+ > Cd2+ similar or equal to Ni2+ and Cd2+ > Pb2+ > Ni2+ similar or equal to Cr3+ for mono-element and multi-element systems, respectively. The mechanisms involved in the adsorption were physisorption, chemisorption, complexation, precipitation, and ion exchange. The presence of other metal ions in the multi-element system caused a synergistic effect on adsorption of Cr3+, Cd2+ and Ni2+ and an antagonistic effect on adsorption of Pb2+. Organosulphur-modified BC can be an effective andselective adsorbent for removing Cd2+, Ni2+, Pb2+ and Cr3+ from aqueous solutions.

SURFACES AND INTERFACES 22, 100822, 2021. DOI: 10.1016/j.surfin.2020.100822

[P056-2021] "Pion-kaon femtoscopy and the lifetime of the hadronic phase in Pb-Pb collisions at root(S)(NN)=2 . 76 TeV"

Acharya, S.; Adamova, D.; Adler, A.; **Albuquerque, D. S. D.*; Chinellato, D. D.*; Takahashi, J.***; et al.; ALICE Collaboration

In this paper, the first femtoscopic analysis of pion-kaon correlations at the LHC is reported. The analysis was performed on the Pb-Pb collision data at root(S)(NN) = 2.76 TeV recorded with the ALICE detector. The non-identical particle correlations probe the spatio-temporal separation between sources of different particle species as well as the average source size of the emitting system. The sizes of the pion and kaon sources increase with centrality, and pions are emitted closer to the centre of the system and/or later than kaons. This is naturally expected in a system with strong radial flow and is qualitatively reproduced by hydrodynamic models. ALICE data on pion-kaon emission asymmetry are consistent with (3+1)-dimensional viscous hydrodynamics coupled to a statistical hadronisation model, resonance propagation, and decay code THERMINATOR 2 calculation, with an additional time delay between 1 and 2 fm/c for kaons. The delay can be interpreted as evidence for a significant hadronic rescattering phase in heavy-ion collisions at the LHC.

PHYSICS LETTERS B 813, 136030, 2021. DOI: 10.1016/j.physletb.2020.136030

[P057-2021] "Production of light-flavor hadrons in pp collisions at root s=7 and root s=13 Tev"

Acharya, S.; Acosta, F. T.; Adam, J.; **Albuquerque, D. S. D.; Chinellato, D. D.*; De Souza, R. D.*; Takahashi, J.***; et al.; ALICE Collaboration

The production of pi(+/-), K-+/-, K-S(0), K*(892)(0), p, phi(1020), Lambda, Xi(-), Omega(-), and their antiparticles was measured in inelastic proton-proton (pp) collisions at a center-of-mass energy of root s = 13 TeV at midrapidity (vertical bar y vertical bar < 0.5) as a function of transverse momentum (P-T) using the ALICE detector at the CERN LHC. Furthermore, the single-particle p(T) distributions of K-S(0), Lambda, and (Lambda) over bar in inelastic pp collisions at root s = 7 TeV are reported here for the first time. The p(T) distributions are studied at midrapidity within the transverse momentum range 0 <= p(T) <= 20 GeV/c, depending on the particle species. The p(T) spectra, integrated yields, and particle yield ratios are discussed as a function of collision energy and compared with measurements at lower root s and with results from various general-purpose QCD-inspired Monte Carlo models. A hardening of the spectra at high p(T) with increasing collision energy is observed, which is similar for all particle species under study. The transverse mass and x(T) 2p(T)/root s scaling properties of hadron produc- tion are also studied. As the collision energy increases from root s = 7-13 TeV, the yields of non- and single-strange hadrons normalized to the pion yields remain approximately constant as a function of root s, while ratios for multi-strange hadrons indicate enhancements.

The p(T)-differential cross sections of pi(+/-), K-+/- and p ((p) over bar) are compared with next-to-leading order perturbative QCD calculations, which are found to overestimate the cross sections for pi(+/-) and p ((p) over bar) at high p(T).

EUROPEAN PHYSICAL JOURNAL C 81[3], 256, 2021. DOI: 10.1140/epjc/s10052-020-08690-5

[P058-2021] "Properties of liquid argon scintillation light emission"

Segreto, E.*

Liquid argon is used as active medium in a variety of neutrino and dark matter experiments thanks to its excellent properties of charge yield and transport and as a scintillator. Liquid argon scintillation photons are emitted in a narrow band of 10 nm centered around 127 nm and with a characteristic time profile made by two components originated by the decay of the lowest lying singlet, (1)Sigma(+)(u), and triplet states, (3)Sigma(+)(u), of the excimer Ar-2* to the dissociative ground state. A model is proposed which takes into account the quenching of the long lived triplet states through the self--interaction with other triplet states or through the interaction with molecular Ar-2(+) ions. The model predicts the time profile of the scintillation signals and its dependence on the intensity of an external electric field and on the density of deposited energy, if the relative abundance of the unquenched fast and slow components is know. The model successfully explains the experimentally observed dependence of the characteristic time of the slow component on the intensity of the applied electric field and the increase of photon yield of liquid argon when doped with small quantities of xenon (at the part per million level). The model also predicts the dependence of the pulse shape parameter, F-prompt, for electron and nuclear recoils on the recoil energy and the behavior of the relative light yield of nuclear recoils in liquid argon, L-eff.

PHYSICAL REVIEW D 103[4], 043001, 2021. DOI: 10.1103/PhysRevD.103.043001

[P059-2021] "Reactor rate modulation oscillation analysis with two detectors in Double Chooz"

Abrahao, T.; Almazan, H.; dos Anjos, J. C.; **Gonzalez, L. F. G.*; Kemp, E.***; et al.; Double Chooz Collaboration

A theta (13) oscillation analysis based on the observed anti-neutrino rates at the Double Chooz far and near detectors for different reactor power conditions is presented. This approach provides a so far unique simultaneous determination of theta (13) and the total background rates without relying on any assumptions on the specific background contributions. The analysis comprises 865 days of data collected in both detectors with at least one reactor in operation. The oscillation results are enhanced by the use of 24.06 days (12.74 days) of reactor--off data in the far (near) detector. The analysis considers the nu <mml:mo stretchy="true"><overbar></mml:mover>e interactions up to a visible energy of 8.5 MeV, using the events at higher energies to build a cosmogenic background model considering fast-neutrons interactions and Li-9 decays. The background-model-independent determination of the mixing angle yields sin(2)(2 theta (13)) = 0.094 0.017, being the best--fit total background rates fully consistent with the cosmogenic background model. A second oscillation analysis is also performed constraining the total background rates to the cosmogenic background estimates. While the central value is not significantly modified due to the consistency between the reactor-off data and the background estimates, the addition of the background model reduces the uncertainty on theta (13) to 0.015. Along with the oscillation results, the normalization of the anti-neutrino rate is measured with a precision of 0.86%, reducing the 1.43% uncertainty associated to the expectation.

JOURNAL OF HIGH ENERGY PHYSICS 1, 190, 2021. DOI: 10.1007/JHEP01(2021)190

[P060-2021] "Reorganization of Resting-State EEG Functional Connectivity Patterns in Children with Cerebral Palsy Following a Motor Imagery Virtual-Reality Intervention"

Stefano Filho, C. A.*; Serrano, J. I.; Attux, R.; **Castellano, G.***; Rocon, E.; del Castillo, M. D.

Motor imagery (MI) has been suggested to provide additional benefits when included in traditional approaches of physical therapy for children with cerebral palsy (CP). Regardless, little is understood about the underlying neurological substrates that might justify its supposed benefits. In this work, we studied resting-state (RS) electroencephalography (EEG) recordings of five children with CP that underwent a MI virtual-reality (VR) intervention. Our aim was to explore functional connectivity (FC) patterns alterations following this intervention through the formalism of graph theory, performing both group and subject-specific analyses. We found that FC patterns were more consistent across subjects prior to the MI-VR intervention, shifting along the anterior-posterior axis, post-intervention, for the beta and gamma bands. Additionally, group FC patterns were not found for the alpha range. Furthermore, intra-subject analyses reinforced the existence of large inter-subject variability and the need for a careful exploration of individual pattern alterations. Such patterns also hinted at a dependency between short-term functional plasticity mechanisms and the EEG frequency bands. Although our sample size is small, we provide a longitudinal analysis framework that can be replicated in future studies, especially at the group level, and whose foundation can be easily extended to verify the validity of our hypotheses.

APPLIED SCIENCES-BASEL 11[5], 2372, 2021. DOI: 10.3390/app11052372

[P061-2021] "Search for dark photons in Higgs boson production via vector boson fusion in proton-proton collisions at root s=13 TeV"

Sirunyan, A. M.; Tumasyan, A.; Adam, W.; **Chinellato, J. A.*; Tonelli Manganote, E. J.*;** et al.; CMS Collaboration

A search is presented for a Higgs boson that is produced via vector boson fusion and that decays to an undetected particle and an isolated photon. The search is performed by the CMS collaboration at the LHC, using a data set corresponding to an integrated luminosity of 130 fb(-1), recorded at a center-of--mass energy of 13 TeV in 2016-2018. No significant excess of events above the expectation from the standard model background is found. The results are interpreted in the context of a theoretical model in which the undetected particle is a massless dark photon. An upper limit is set on the product of the cross section for production via vector boson fusion and the branching fraction for such a Higgs boson decay, as a function of the Higgs boson mass. For a Higgs boson mass of 125 GeV, assuming the standard model production rates, the observed (expected) 95% confidence level upper limit on the branching fraction is 3.5 (2.8)%. This is the first search for such decays in the vector boson fusion channel. Combination with a previous search for Higgs bosons produced in association with a Z boson results in an observed (expected) upper limit on the branching fraction of 2.9 (2.1)% at 95% confidence level.

JOURNAL OF HIGH ENERGY PHYSICS 3, 011, 2021. DOI: 10.1007/JHEP03(2021)011

[P062-2021] "Search for new physics in top quark production with additional leptons in proton-proton collisions at root s=13 TeV using effective field theory"

Sirunyan, A. M.; Tumasyan, A.; Adam, W.; **Chinellato, J. A.*; Tonelli Manganote, E. J.***; et al.; CMS Collaboration

Events containing one or more top quarks produced with additional prompt leptons are used to search for new physics within the framework of an effective field theory (EFT). The data correspond to an integrated luminosity of 41.5 fb(-1) of proton-proton collisions at a center-of-mass energy of 13 TeV at the LHC, collected by the CMS experiment in 2017. The selected events are required to have either two leptons with the same charge or more than two leptons; jets, including identified bottom quark jets, are also required, and the selected events are divided into categories based on the multiplicities of these objects. Sixteen dimension-six operators that can affect processes involving top quarks produced with additional charged leptons are considered in this analysis. Constructed to target EFT effects directly, the analysis applies a novel approach in which the observed yields are parameterized in terms of the Wilson coefficients (WCs) of the EFT operators. A simultaneous fit of the 16 WCs to the data is performed and two standard deviation confidence intervals for the WCs are extracted; the standard model expectations for the WC values are within these intervals for all of the WCs probed.

JOURNAL OF HIGH ENERGY PHYSICS 3, 095, 2021. DOI: 10.1007/JHEP03(2021)095

[P063-2021] "Search for the lepton flavor violating decay tau -> 3 mu in proton-proton collisions at root s=13 TeV"

Sirunyan, A. M.; Tumasyan, A.; Adam, W.; **Chinellato, J. A.*; Tonelli Manganote, E. J.***; et al.; CMS Collaboration

Results are reported from a search for the lepton flavor violating decay tau -> 3 mu in proton-proton collisions at root s = 13 TeV. The data sample corresponds to an integrated luminosity of 33.2 fb(-1) recorded by the CMS experiment at the LHC in 2016. The search exploits tau leptons produced in both W boson and heavy-flavor hadron decays. No significant excess above the expected background is observed. An upper limit on the branching fraction B(tau -> 3 mu) of 8.0 x 10(-8) at 90% confidence level is obtained, with an expected upper limit of 6.9 x 10(-8).

JOURNAL OF HIGH ENERGY PHYSICS 1, 163, 2021. DOI: 10.1007/JHEP01(2021)163

[P064-2021] "Selecting 'convenient observers' to probe the atomic structure of CVD graphene on Ir(111) via photoelectron diffraction"

Barreto, L.; Lima, L. H. de; Martins, D. C.; **Silva, C.*; Ferreira, R. C. C. de*; Landers, R.*; Siervo, A. de***

CVD graphene grown on metallic substrates presents, in several cases, a long-range periodic structure due to a lattice mismatch between the graphene and the substrate. For instance, graphene grown on Ir(111), displays a corrugated supercell with distinct adsorption sites due to a variation of its local electronic structure. This type of surface reconstruction represents a challenging problem for a detailed atomic surface structure determination for experimental and theoretical techniques. In this work, we revisited the surface structure determination of graphene on Ir(111) by using the unique advantage of surface and chemical selectivity of synchrotron-based photoelectron diffraction. We take advantage of the Ir 4f photoemission surface state and use its diffraction signal as a probe to investigate the atomic arrangement of the graphene topping layer. We determine the average height and the overall corrugation of the graphene layer, which are respectively equal to 3.40 +/- 0.11 angstrom and 0.45 +/- 0.03 angstrom. Furthermore, we explore the graphene topography in the vicinity of its high-symmetry adsorption sites and show that the experimental data can be described by three reduced systems simplifying the moire supercell multiple scattering analysis.

JOURNAL OF PHYSICS-CONDENSED MATTER 33[10], 105001, 2021. DOI: 10.1088/1361-648X/abceff

[P065-2021] "Semi-device-independent certification of entanglement in superdense coding"

Moreno, G.; Nery, R.; **Gois, C. de*; Rabelo, R.***; Chaves, R.

Superdense coding is a paradigmatic protocol in quantum information science, employing a quantum communication channel to send classical information more efficiently. As we show here, it can be understood as a particular case of a prepare and measure experiment, a scenario that has attracted growing attention for its fundamental and practical applications. Formulating superdense coding as a prepare and measure scenario allows us to provide a semi-device-independent witness of entanglement that significantly improves over previous tests. Furthermore, we also show how to adapt our results into self-testing of maximally entangled states and also provide a semidefinite program formulation allowing one to efficiently optimize, for any shared quantum state, the probability of success in the superdense coding protocol.

PHYSICAL REVIEW A 103[2], 022426, 2021. DOI: 10.1103/PhysRevA.103.022426

[P066-2021] "SiPM-matrix readout of two-phase argon detectors using electroluminescence in the visible and near infrared range"

Aalseth, C. E.; Abdelhakim, S.; Agnes, P.; **Machado, A. A.*; Segreto, E.***; et al.; DarkSide-20K Collaboration

Proportional electroluminescence (EL) in noble gases is used in two-phase detectors for dark matter searches to record (in the gas phase) the ionization signal induced by particle scattering in the liquid phase. The "standard" EL mechanism is considered to be due to noble gas excimer emission in the vacuum ultraviolet (VUV). In addition, there are two alternative mechanisms, producing light in the visible and near infrared (NIR) ranges. The first is due to bremsstrahlung of electrons scattered on neutral atoms ("neutral bremsstrahlung", NBrS). The second, responsible for electron avalanche scintillation in the NIR at higher electric fields, is due to transitions between excited atomic states. In this work, we have for the first time demonstrated two alternative techniques of the optical readout of two-phase argon detectors, in the visible and NIR range, using a silicon photomultiplier matrix and electroluminescence due to either neutral bremsstrahlung or avalanche scintillation. The amplitude yield and position resolution were measured for these readout techniques, which allowed to assess the detection threshold for electron and nuclear recoils in two-phase argon detectors for dark matter searches. To the best of our knowledge, this is the first practical application of the NBrS effect in detection science.

EUROPEAN PHYSICAL JOURNAL C 81[2], 153, 2021. DOI: 10.1140/epjc/s10052-020-08801-2

[P067-2021] "Spectral characteristics of subthalamic nucleus local field potentials in Parkinson's disease: Phenotype and movement matter"

Godinho, F.; **Fim Neto, A.***; Bianqueti, B. L.; Luccas, J. B. de; Varjao, E.; Terzian Filho, P. R.; Figueiredo, E. G.; Almeida, T. P.; Yoneyama, T.; Takahata, A. K.; Rocha, M. S.; Soriano, D. C.

Parkinson's disease (PD) is clinically heterogeneous across patients and may be classified in three motor phenotypes: tremor dominant (TD), postural instability and gait disorder (PIGD), and undetermined. Despite the significant clinical characterization of motor phenotypes, little is known about how electrophysiological data, particularly subthalamic nucleus local field potentials (STN-LFP), differ between TD and PIGD patients. This is relevant since increased STN-LFP bandpower at alpha-beta range (8-35 Hz) is considered a potential PD biomarker and, therefore, a critical setpoint to drive adaptive deep brain stimulation. Acknowledging STN-LFP differences between phenotypes, mainly in rest and movement states, would better fit DBS to clinical and motor demands. We studied this issue through spectral analyses on 35 STN-LFP in TD and PIGD patients during rest and movement. We demonstrated that higher beta(2) activity (22-35 Hz) was observed in PIGD only during rest. Additionally, bandpower differences between rest and movement occurred at the alpha-beta range, but with different patterns as per phenotypes: movement-induced desynchronization concerned lower frequencies in TD (10-20 Hz) and higher frequencies in PIGD patients (21-28 Hz). Finally, when supervised learning algorithms were employed aiming to discriminate PD phenotypes based on STN-LFP bandpower features, movement information had improved the classification accuracy, achieving peak performances when TD and PIGD movement-induced desynchronization ranges were considered. These results suggest that STN-LFP beta-band encodes phenotype-movement dependent information in PD patients.

EUROPEAN JOURNAL OF NEUROSCIENCE, 2021. DOI: 10.1111/ejn.15103

[P068-2021] "Stoichiometry and Orientation- and Shape--Mediated Switching Field Enhancement of the Heating Properties of Fe3O4 Circular Nanodiscs"

Niraula, G.; Coaquira, J. A. H.; Aragon, F. H.; Bakuzis, A. F.; Villar, B. M. G.; Garcia, F.; **Muraca, D.***; Zoppellaro, G.; Ayesh, A.; Sharma, S. K.

The generation of topological magnetic vortex-domain structures in iron-oxide nanomaterials has promising applications in biomedical scenarios, such as heat generators for hyperthermia treatments. In this report we describe alternative kinds of magnetic-vortex nanoparticles, circular Fe nanodiscs (NDs), and dissect their heating properties by in-depth investigation of their shape and size, stoichiometry, orientations, and switching field "H" behaviors, through experiments and theoretical simulation. We find that the stoichiometric NDs show better heating performance than nonstoichiometric materials because of the significant electron hopping between Feand Fe ion. The higher heating efficiency (in terms of specific absorption rate, SAR) is observed only for the higher switching field regime, an effect that is associated with the parallel and perpendicular alignment of nanodiscs with respect to low and high ac magnetic field, respectively. A higher SAR of approximately 270 W/g is observed at a higher switching field (approximately 700 Oe) for NDs of diameter 770 nm, which increases by a factor of 4 at a switching field of approximately 360 Oe for NDs of diameter 200 nm. The reported results suggest that the heating efficiency in these systems can be enhanced by controlling the switching field, which is, in turn, tuned by size, shape, and orientation of circular magnetic vortex nanodiscs.

PHYSICAL REVIEW APPLIED 15[1], 014056, 2021. DOI: 10.1103/PhysRevApplied.15.014056

[P069-2021] "Structure, Mechanical Properties and Oxidation Resistance of Iso and Non-Iso Architected TiN/Cr Multilayers Coatings Deposited by Magnetron Sputtering"

Soares, V. F. G.; Ramirez, D. A.; Damasceno, I. Z.; **Echevirrigaray, F. G.*;** Figueroa, C. A.; Perotti, B. L.; Serafini, F. L.; Oliveira, G. B.; Terto, A. R.; Tentardini, E. K.

Iso and non-iso architected TiN/Cr multilayers with constant composition were deposited by balanced magnetron sputtering aiming to investigate the influence of different architectures over coatings structures and properties. Glow discharge optical emission spectroscopy analyses were used to determine in-depth constituents and suggested that no diffusion of elements occurred between layers in room temperature. Field emission gun scanning electron microscopy analyses showed that all multilayers presented sharp interfaces and low porosity microstructures, with column-like grain growth influenced by layer sizes. Glancing angle X-ray diffraction analyses showed that multilayers consist of polycrystalline alpha-Cr and delta-TiN phases with a main peak in Cr(110) plane. The overlapping of TiN onto metallic layers led to the suppression of growth in the TiN(111) plane, although TiN layers thicker than 50 nm demonstrated a growth in plane TiN(200). Nanoindentation tests registered equal hardness values for all multilayers of around 16.2 GPa, on the other hand, a tendency to improve hardness has been identified for hierarchical multilayer. Oxidation tests revealed that architectures with thicker TiN top layers presented an improved oxidation resistance up to 600 degrees C, probably due to growth in more compact TiN(200) plane. However, TiN/Cr coatings did not resist integrally to oxidation tests at 750 degrees C.

MATERIALS RESEARCH-IBERO-AMERICAN JOURNAL OF MATERIALS 24[1], e20200315, 2021. DOI: 10.1590/1980-5373-MR-2020-0315

[P070-2021] "Studies of charm and beauty hadron long-range correlations in pp and pPb collisions at LHC energies"

Sirunyan, A. M.; Tumasyan, A.; Adam, W.; **Chinellato, J. A.*; Tonelli Manganote, E. J.*;** et al.; CMS Collaboration

Measurements of the second Fourier harmonic coefficient (v(2)) of the azimuthal distributions of prompt and nonprompt D-0 mesons produced in pp and pPb collisions are presented. Nonprompt D-0 mesons come from beauty hadron decays. The data samples are collected by the CMS experiment at nucleon--nucleon center-of-mass energies of 13 and 8.16 TeV, respectively. In high multiplicity pp collisions, v(2) signals for prompt charm hadrons are reported for the first time, and are found to be comparable to those for light-flavor hadron species over a transverse momentum (pT) range of 2-6 GeV. Compared at similar event multiplicities, the prompt D-0 meson v(2) values in pp and pPb collisions are similar in magnitude. The v(2) values for open beauty hadrons are extracted for the first time via nonprompt D-0 mesons in pPb collisions. For pT in the range of 2-5 GeV, the results suggest that v(2) for nonprompt D-0 mesons is smaller than that for prompt D-0 mesons. These new measurements indicate a positive charm hadron v(2) in pp collisions and suggest a mass dependence in v(2) between charm and beauty hadrons in the pPb system. These results provide insights into the origin of heavy-flavor quark collectivity in small systems.

PHYSICS LETTERS B 813, 136036, 2021. DOI: 10.1016/j.physletb.2020.136036

[P071-2021] "The very forward CASTOR calorimeter of the CMS experiment"

Khachatryan, V.; Sirunyan, A. M.; Tumasyan, A.; **Chinellato, J. A.*; Tonelli Manganote, E. J.***; et al.; CMS Collaboration

The physics motivation, detector design, triggers, calibration, alignment, simulation, and overall performance of the very forward CASTOR calorimeter of the CMS experiment are reviewed. The CASTOR Cherenkov sampling calorimeter is located very close to the LHC beam line, at a radial distance of about 1 cm from the beam pipe, and at 14.4 m from the CMS interaction point, covering the pseudorapidity range of -6.6 < eta < - 5.2. It was designed to withstand high ambient radiation and strong magnetic fields. The performance of the detector in measurements of forward energy density, jets, and processes characterized by rapidity gaps, is reviewed using data collected in proton and nuclear collisions at the LHC.

JOURNAL OF INSTRUMENTATION 16[2], P02010, 2021. DOI: 10.1088/1748-0221/16/02/P02010

[P072-2021] "Thermally Reduced Soft Magnetic CuFe Nanoparticles for High-Performance Electrical Devices"

Prabhakaran, T.*; Mangalaraja, R. V.; **Beron, F.***; Jimenez, J. A.; Denardin, J. C.; Arun, T.; Akbari-Fakhrabadi, A.

Developing economically soft magnetic materials for high-performance electrical devices is indispensable. Here, we present the structural and magnetic properties of thermally reduced soft CuFe nanoparticles. The fcc cubic structure of iron-rich Cu37Fe63 and their composition was confirmed by Rietveld refinement. Cu37Fe63 nanoparticles exhibited high saturation magnetization and coercivity of 127 emu/g (142 emu/g) and 43 Oe (31 Oe), respectively, at 300 K (5 K). They showed transitions at similar to 34 and similar to 249 K due to the Kondo temperature of CuFe and minor fraction of CuFe2O4, respectively. The exchange coupling between Cu and Fe was not significant, as demonstrated by field-cooled magnetization curves at 5 K. The magnetocaloric effect (MCE) in the range of fields and temperatures was estimated whereas the maximum MCE of -8.71 x 10(-2) J.kg(-1).K-1 was achieved at 222 K. These soft magnetic materials, which exhibited stable high saturation magnetization with less heating effect during magnetization and demagnetization cycles, would he suitable candidates for magnetic applications.

IEEE TRANSACTIONS ON MAGNETICS 57[2], 2000306, 2021. DOI: 10.1109/TMAG.2020.3042130

[P073-2021] "Thiophene-Tetrathia-Annulene monolayer (TTA-2D): A new 2D semiconductor material with indirect bandgap"

Tromer, R. M.*; Machado, L. D.; Woellner, C. F.; **Galvão, D. S.***

We propose a new 2D semiconductor material (TTA-2D) based on the molecular structure of ThiopheneTetrathia-Annulene (TTA). The TTA-2D structural, electronic, and optical properties were investigated ab initio methods. Our results show that TTA-2D is a small indirect bandgap semiconductor (0.6 semiconductor-metal transition can be induced by applying a uniaxial strain. Our results also show that is thermally stable up to T = 1000 K. TTA-2D absorbs in a large spectral range, from infrared to ultraviolet regions. Values of refractive index and reflectivity show that TTA-2D reflects only 10% of the incident light visible region. These results suggest that TTA-2D is a promising material for solar cell applications.

PHYSICA E-LOW-DIMENSIONAL SYSTEMS & NANOSTRUCTURES 129, 114586, 2021. DOI: 10.1016/j.physe.2020.114586

[P074-2021] "Toward Waveguide-Based Optical Chromatography"

Neves, A. A. R.; Moreira, W. L.; Fontes, A.; Euser, T. G.; **Cesar, C. L.***

We report analytical expressions for optical forces acting on particles inside waveguides. The analysis builds on our previously reported Fourier Transform method to obtain Beam Shape Coefficients for any beam. Here we develop analytical expressions for the Beam Shape Coefficients in cylindrical and rectangular metallic waveguides. The theory is valid for particle radius a ranging from the Rayleigh regime to large microparticles, such as aerosols like virus loaded droplets. The theory is used to investigate how optical forces within hollow waveguides can be used to sort particles in "optical chromatography" experiments in which particles are optically propelled along a hollow-core waveguide. For Rayleigh particles, the axial force is found to scale with a (6), while the radial force, which prevents particles from crashing into the waveguide walls, scales with a (3). For microparticles, narrow Mie resonances create a strong wavelength dependence of the optical force, enabling more selective sorting. Several beam parameters, such as power, wavelength, polarization state and waveguide modes can be tuned to optimize the sorting performance. The analysis focuses on cylindrical waveguides, where meter-long liquid waveguides in the form of hollow-core photonic crystal fibers are readily available. The modes of such fibers are well-approximated by the cylindrical waveguide modes considered in the theory.

FRONTIERS IN PHYSICS 8, 603641, 2021. DOI: 10.3389/fphy.2020.603641

[P075-2021] "Transverse-momentum and event-shape dependence of D-meson flow harmonics in Pb-Pb collisions at root(S)(NN)=5 . 02 TeV"

Acharya, S.; Adamova, D.; Adler, A.; **Albuquerque, D. S. D.*; Chinellato, D. D.*; Takahashi, J.***; et al.; ALICE Collaboration

The elliptic and triangular flow coefficients v(2) and v(3) of prompt D-0 , D+ , and D*(+) mesons were measured at midrapidity (|y| < 0.8) in Pb-Pb collisions at the centre-of-mass energy per nucleon pair of root(S)(NN) = 5.02 TeV with the ALICE detector at the LHC. The D mesons were reconstructed via their hadronic decays in the transverse momentum interval 1 < p(T) < 36 GeV/c in central (0-10%) and semi-central (30-50%) collisions. Compared to pions, protons, and J/psi mesons, the average D-meson v(n) harmonics are compatible within uncertainties with a mass hierarchy for p(T) less than or similar to 3 GeV/c , and are similar to those of charged pions for higher p(T). The coupling of the charm quark to the light quarks in the underlying medium is further investigated with the application of the event-shape engineering (ESE) technique to the D-meson v(2) and p(T)-differential yields. The D-meson v(2) is correlated with average bulk elliptic flow in both central and semi-central collisions. Within the current precision, the ratios of per-event D meson yields in the ESE--selected and unbiased samples are found to be compatible with unity. All the measurements are found to be reasonably well described by theoretical calculations including the effects of charm-quark transport and the recombination of charm quarks with light quarks in a hydrodynamically expanding medium.

PHYSICS LETTERS B 813, 136054, 2021. DOI: 10.1016/j.physletb.2020.136054

[P076-2021] "Ultrafast dynamics of carriers and phonons of photoinjected double-plasma in aluminium nitride"

Rodrigues, C. G.; **Luzzi, R.***

Aluminum nitride is attracting great interest of the industry and scientific community due to its interesting properties. In this paper is performed a theoretical study on the ultrafast transient transport properties of photoinjected carriers in wurtzite AlN subjected to electric fields up to 80 kV/cm.

For this, the Nonequilibrium Statistical Operator Method was used. The evolution towards the steady state of drift velocity of carriers (electrons and holes) and nonequilibrium temperature (carriers and phonons) subpicosecond scale were determined.

REVISTA MEXICANA DE FISICA 67[2], 318-323, 2021. DOI: 10.31349/RevMexFis.67.318

[P077-2021] "Zinc (II) modified hydroxyapatites for tetracycline removal: Zn (II) doping or ZnO deposition and their influence in the adsorption"

Oliveira, C.; Oliveira, A. L. M. de; Chantelle, L.; **Landers, R.*;** Medina-Carrasco, S., Orta, M. D.; Silva Filho, E. C.; Fonseca, M. G.

Zn(II) modified hydroxyapatites were prepared through the microwave-assisted co-precipitation/hydrothermal method using zinc acetate and HAp in the presence of casein as the template, followed by calcination at 500 degrees C in an oxygen atmosphere with the heating rate of 2 degrees C min(-1) for 12 h. The zinc acetate proportion in relation to the mass of pure HAp was varied to obtain theoretical final products with 5%, 10%, and 20% ZnO, which were labeled as HAp/ZnO-1, HAp/ZnO-2, and HAp/ZnO-3, respectively. The synthesized solids were then characterized using X-ray diffraction, Fourier transform infrared spectroscopy, Raman spectroscopy, X-ray photoelectron spectroscopy, scanning electron microscopy, transmission electron microscopy, X-ray dispersive spectroscopy, and nitrogen adsorption/desorption isotherm measurements. The adsorptive properties of the materials for the removal of tetracycline (TC) from aqueous solutions were evaluated using the Langmuir, Freundlich, and Temkin isotherm models. The structural characterizations revealed the formation of Zn-doped HAp/ZnO--type composites. The samples rich in ZnO (HAp/ZnO-3) exhibited good TC removal efficiency with a maximum adsorption of 168.5 mg L-1 within 20 min. The adsorption capacity data of the samples could be well-fitted to the Langmuir model. The ZnO content played an important role in adjusting the adsorptive properties of HAp for applications in wastewater treatment, especially for the removal of drugs from aqueous solutions.

POLYHEDRON 194, 114879, 2021. DOI: 10.1016/j.poly.2020.114879

Artigos aceitos para publicação

[A001-2021] "How Crystallization Affects the Oriented Attachment of Silver Nanocrystals"

Faccin, G. M.*; Pereira, Z. S.; **Silva, E. Z. da***

Oriented attachment processes between nanocrystals provide a promising route for the synthesis of mesocrystals that, although made of the same elements as their usual crystal counterparts, nevertheless possess very distinct physical and chemical properties that can be explored for technological applications. In this study, the oriented attachment process experimentally observed between silver nanocrystals is analyzed through a systematic approach involving a series of molecular dynamics simulations. The simulations elucidate how the crystallization process between silver nanocrystals leads to either imperfect oriented attachment or perfect oriented attachment, how likely those processes are to occur and how faceting affects their outcome. This information can be explored to develop new strategies aimed at triggering specific crystallization processes that take place during mesocrystal growth, thus allowing control over the characteristics of the final synthesized material.

THE JOURNAL OF PHYSICAL CHEMISTRY C 125[12], 6812-6820, 2021. DOI: 10.1021/acs.jpcc.0c10321 **(Artigo destaque de capa)**

Correções

[Co003-2021] "Experimental Study on Glass and Polymers: Determining the Optimal Material for Potential Use in Terahertz Technology (vol 8, pg 97204, 2020)"

Islam, M. S.; **Cordeiro, C. M. B.***; Nine, M. J.; Sultana, J.; Cruz, A. L. S.; Dinovitser, A.; Ng, B. W. H.; Heidepriem, H. E.; Losic, D.; Abbott, D.
Fig. 4 in reference [1] is after [2].

IEEE ACCESS 9, 2705-2705, 2021. DOI: 10.1109/ACCESS.2020.3047311

[Co004-2021] "Terahertz Hollow Core Antiresonant Fiber with Metamaterial Cladding (vol 8, 14, 2020)"

Sultana, J.; Islam, M. S.; **Cordeiro, C. M. B.***; Dinovitser, A.; Kaushik, M.; Ng, B. W. H.; Abbott, D.

FIBERS 9[3], 20, 2021. DOI: 10.3390/fib9030020

[Co005-2021] "Tunable localized surface plasmon graphene metasurface for multiband superabsorption and terahertz sensing (vol 158, pg 559, 2020)"

Islam, M. S.; Sultana, J.; Biabanifard, M.; Vafapour, Z.; Nine, M. J.; Dinovitser, A.; **Cordeiro, C. M. B.*;** Ng, B. W. -H.; Abbott, D.

CARBON 174, 770-770, 2021. DOI: 10.1016/j.carbon.2020.12.087

***Autores da comunidade IFGW**
Fonte: Web of Science on-line (WOS)

Defesas de Dissertações do IFGW

[D003-2021] "Optimized Vivid Color and Tunable Grating Plasmonic Reflector"
Aluno: Ana Luisa Amadeu Ribeiro
Orientador: Prof. Dr. Thiago Pedro Mayer Alegre
Data: 10/03/2021

[D004-2021] "Estudo de sinais de raios cósmicos em um detector de radiação Cherenkov em água"
Aluno: Renan de Aguiar
Orientador: Prof. Dr. Anderson Campos Fauth
Data: 26/03/2021

[D005-2021] "Ondas gravitacionais e o espaço-tempo de Robinson-Trautman"
Aluno: Paulo Sergio Piva
Orientador: Prof. Dr. Alberto Vazquez Saa
Data: 31/03/2021

[D006-2021] "Decaimento do píon carregado baseado em um modelo SU(3) X SU(3) X U(1)"
Aluno: Leonardo José Ferreira Leite
Orientador: Prof. Dr. Marcelo Moraes Guzzo
Data: 07/04/2021

[D007-2021] "Compatibilidade de medições em testes de não-localidade de Bell"
Aluno: Gabriel Ruffolo
Orientador: Prof. Dr. Rafael Luiz da Silva Rabelo
Data: 08/04/2021

[D008-2021] "Novos critérios para o princípio da causalidade de informação"
Aluno: Lucas da Silva Pollyceno
Orientador: Prof. Dr. Rafael Luiz da Silva Rabelo
Data: 09/04/2021

Fonte: Portal IFGW/Pós-graduação - Agenda de Colóquios, Defesas e Seminários.
Disponível em: http://portal.ifi.unicamp.br/pos-graduacao

Defesas de Teses do IFGW

[T002-2021] "Interação dos estados da matéria com o meio: ondas mecânicas"
Aluno: Helder Faria Andriolo
Orientador: Prof. Dr. José Antônio Brum
Data: 02/02/2021

[T003-2021] "BUSCA DE DECAIMENTOS RAROS EM SABORES PESADOS NO EXPERIMENTO CMS/LHC/CERN"
Aluno: Felipe Torres da Silva de Araujo
Orientador: Prof. Dr. José Augusto Chinellato
Data: 20/04/2021

Fonte: Portal IFGW/Pós-graduação - Agenda de Colóquios, Defesas e Seminários.
Disponível em: http://portal.ifi.unicamp.br/pos-graduacao

Defesas de Teses e Dissertações do PECIM

[Pe001-2021] "EXAME DE QUALIFICAÇÃO - ELEMENTOS HISTÓRICOS E FILOSÓFICOS DA CIÊNCIA NA FORMAÇÃO INICIAL DE PROFESSORES: uma investigação a partir das provas de ENADE de 2017 dos cursos de licenciatura em ciências e matemática"
Aluno: Ivy Judensnaider
Orientador: Profa. Dra. Silvia Fernanda de Mendonça Figueirôa
Data: 20/04/2021
Exame de Defesa: Doutorado
Banca: Profa. Dra. Silvia Fernanda de Mendonça Figueirôa (orient.), Profa. Dra. Elisabete Monteiro de Aguiar Pereira - FE /Unicamp, **Prof. Dr. Mauricio Urban Kleinke - IFGW / UNICAMP,** Prof. Dra. Maria José Fontana Gebara - UFSCAR, suplente, Prof. Dr. Dario Fiorentini - FE /Unicamp, suplente

Fonte: Página do Programa de Pós-Graduação Multiunidades em Ensino de Ciências e Matemática – Mestrado e Doutorado (PECIM) **- Disponível em:** https://www.pecim.unicamp.br/bancas

Abstracta

Instituto de Física
Diretor: Prof. Dr. Pascoal José Giglio Pagliuso
Diretora Associada: Profa. Dra. Mônica Alonso Cotta
Universidade Estadual de Campinas - UNICAMP
Cidade Universitária Zeferino Vaz
13083-859 - Campinas - SP - Brasil
e-mail: secdir@ifi.unicamp.br
Fone: +55 19 3521-5300

Publicação

Biblioteca do Instituto de Física Gleb Wataghin
http://portal.ifi.unicamp.br/biblioteca

Diretora Técnica: Sandra Maria Carlos Cartaxo
Coordenadora da Comissão de Biblioteca: Profa. Dra. Arlene Cristina Aguilar

Elaboração:
Maria Graciele Trevisan (Bibliotecária)
Ayres Neri da Cunha Junior (Técnico Administrativo)
contato: infobif@ifi.unicamp.br